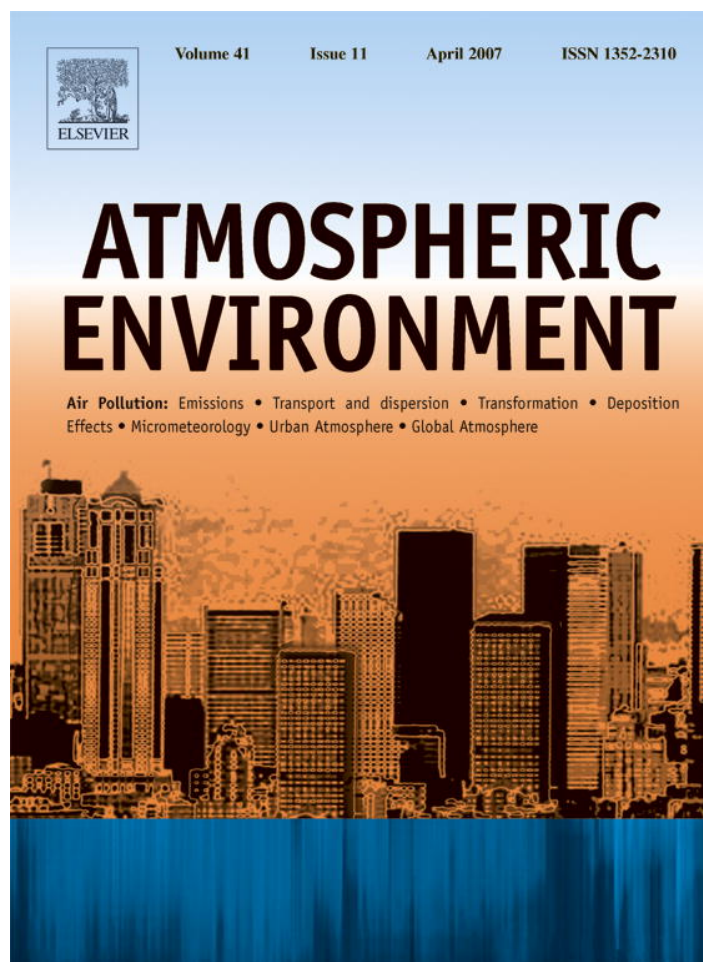


Provided for non-commercial research and educational use only.
Not for reproduction or distribution or commercial use.



This article was originally published in a journal published by Elsevier, and the attached copy is provided by Elsevier for the author's benefit and for the benefit of the author's institution, for non-commercial research and educational use including without limitation use in instruction at your institution, sending it to specific colleagues that you know, and providing a copy to your institution's administrator.

All other uses, reproduction and distribution, including without limitation commercial reprints, selling or licensing copies or access, or posting on open internet sites, your personal or institution's website or repository, are prohibited. For exceptions, permission may be sought for such use through Elsevier's permissions site at:

<http://www.elsevier.com/locate/permissionusematerial>

Chemical segregation by heterogeneous emissions

Ludovic Auger^{a,*}, Bernard Legras^b

^aCentre National de Recherches Météorologiques, URA 1357, Météo France, Toulouse, France

^bLaboratoire de Météorologie Dynamique, UMR 8539, Ecole Normale Supérieure, Paris, France

Received 13 July 2006; received in revised form 26 October 2006; accepted 7 November 2006

Abstract

Ozone pollution in the boundary layer results from photoactivated chemistry of primary pollutants released at the ground. As emissions are highly inhomogeneous in space and time and some chemical time-scales are of the order or larger than dynamical time-scales, it is admitted that turbulent transport and mixing is a key factor in ozone production. We study the interaction between chemistry and convective boundary layer turbulent with a large eddy simulation model coupled to CHIMERE, a detailed chemical model, over a 10×10 km domain. Our results show that when emissions are concentrated over a limited area, strong values of segregation between chemical species are obtained over the first two active hours during the morning, leading to significant impact in terms of pollutants concentration. After 3 h, for each heterogeneous emission case considered, segregation drops to a few percents for most compounds pairs, due to the strong convective mixing of the boundary layer.

© 2006 Elsevier Ltd. All rights reserved.

Keywords: Atmospheric chemistry; LES; Boundary layer; Segregation; Turbulence

1. Introduction

Ozone pollution events are associated with warm and sunny weather which enhances the photochemistry required for ozone production. A common assumption of most models of urban pollution is that all the pollutants released at the surface are rapidly distributed by convection within the boundary layer where they mix and react together and with other species already present. However, as the main sources due to traffic or industry are highly heterogeneous in their spatial distribution, the question arises of how long the heterogeneities

are preserved within the flow and how much this influences the chemistry. This question is an important component of the more general problem of understanding the interaction between the chemistry and the small-scale dynamics in the boundary layer and of how to parametrize it in large-scale chemistry transport models.

Under sunny summer conditions, a well-mixed convective boundary layer (CBL) establishes from mid-morning to the end of the day. It is characterized by a positive heat flux ($\overline{w'\theta'_0} > 0$) and an approximately uniform potential temperature profile. An important parameter for chemistry is the height z_i of the CBL which increases during the day and can reach up to 4000 m depending of the meteorological conditions. The CBL displays an intermittent structure composed of turbulent updraft and downdraft

*Corresponding author.

E-mail addresses: ludovic.auger@meteo.fr (L. Auger), legras@lmd.ens.fr (B. Legras).

plumes extending across its depth with a horizontal length scale of the order of 100 m (Kaimal and Businger, 1970; Wilczak and Businger, 1983). Up-draft plumes are carrying the pollutants from the surface and distribute them within the CBL. As the characteristic time-scales of these plumes is a few minutes, which is akin to the time-scale of ozone chemistry, we can expect important interactions between turbulence and chemistry.

The first approach to evaluate the role of turbulence for reactive species, is to apply closure assumptions on turbulent fluxes. Gao and Wesely (1994) used a second order closure and showed that the profiles for reacting NO_2 , NO_3 and N_2O_5 differ from the profile of an inert tracer. Similar results have been obtained in the case of neutral or stratified boundary layer (Galmarini et al., 1995, 1997). Vilà-Guerau de Arellano and Duynkerke (1995), extending the similarity theory of Monin–Obukhov to reactive species, showed for a near-neutral boundary layer that the deviation from the flux-gradient relation is very large for the less abundant species and Petersen (2000) compared first and higher order closures. In these studies, the turbulent closures are parametrized as a function of Damköhler numbers and emission ratios.

A second approach is to perform detailed calculations based on large eddy simulations (LES) in order to compute explicitly advection and chemical reactions over a wide domain. This technique was first used by Schuman (1989) and Sykes et al. (1994) who showed a strong effect for fast reactions. More recent LES simulations (Vinuesa and Vilà-Guerau de Arellano, 2003) with a second order chemical reaction showed that the fluxes and covariances could be less affected by chemistry when the chemical species are in equilibrium. Krol et al. (2000), using a more complex chemistry, investigated the influence of non-uniform emissions inside the domain and found that some reactions could be slowed down by as much as 30% compared to a box model. The same chemistry was used by Vinuesa and Vilà-Guerau de Arellano (2005) to test a subgrid-scale parametrization against LES simulations.

It is, however, difficult to assess the influence of turbulent fluctuations in a realistic urban pollution environment as all previous studies have been performed with highly simplified chemistry. The goal of this study is to analyse the interaction of CBL turbulent fluctuations with a realistic, state-of-the-art, chemical model. We couple a LES simula-

tion based on a model by Moeng (1984), and the CHIMERE chemical model (Vautard et al., 2001) which is currently used for operational forecast of air pollution over France and western Europe (Schmidt et al., 2001). The coupled model is ran on a 10×10 km domain with a grid size of 125 m that resolves explicitly the most energetic eddies.

In Section 2, we describe the dynamical and the chemical components of the coupled model. Section 3 describes a reference experiment with uniform emissions and discusses the factors influencing segregation. In Section 4, we study the impact of inhomogeneous emissions at the ground, intended to mimic the effect of heavy polluting areas such as roads or industrial zones neighbour to less polluted areas. Section 5 offers a summary and discussion.

2. Description of the coupled model

2.1. Dynamical component

LES has been used to model the atmospheric boundary layer since the pioneering work of Deardorff (1972). We follow here the developments described in Moeng (1984) which are known to be accurate for convective conditions. An LES is based on spatial filtering of the equation of motion to retain only contributions that can be represented at a given resolution, and on parametrizing the subgrid terms. Spatial filtering is performed through a horizontal average

$$\langle \mathcal{T} \rangle(x) = \int_D G(x - x') \mathcal{T}(x') dx', \quad (1)$$

where the filtering function is chosen as $G = (\sqrt{\pi}/\gamma/2 dI) \exp[-(\sqrt{\gamma}/2 dI)^2 x^2]$ with $\gamma = 6$ and dI is the grid size of the model.

The boundary conditions are chosen periodic in x and y . The vertical direction is discretized between 0 and 1600 m with 64 levels separated by 25 m increments using a staggered grid such that levels for θ and w are interleaved. Most of our experiments have been performed within a horizontal domain of 10×10 km with 80×80 grid points corresponding to a horizontal grid resolution of 125 m.

The subgrid-scale parametrization, is based on Smagorinsky nonlinear eddy-viscosity (Smagorinsky, 1963) in which the subgrid kinetic energy is derived from an empirical equation (Deardorff, 1980). From the kinetic energy we draw the eddy coefficients for momentum (K_M) and heat (K_H), and

we compute the subgrid-scale (SGS) stresses for momentum and heat as

$$\tau_{ij} = -K_M \left(\frac{\partial \langle u \rangle_i}{\partial x_j} + \frac{\partial \langle u \rangle_j}{\partial x_i} \right), \quad (2)$$

$$\tau_{\theta i} = -K_H \frac{\partial \langle \theta \rangle}{\partial x_i}. \quad (3)$$

The surface momentum SGS flux is estimated from extrapolating the values at the first level through logarithmic similarity. The surface SGS heat flux is calculated so that the total surface heat flux is equal to a prescribed boundary distribution. The boundary conditions at the top level are $w = 0$ and zero SGS fluxes. We also impose a strongly stratified layer just above the CBL which damps vertical motion aloft.

In order to validate our LES code, we have simulated a well documented case of clear sky convective situation, namely day 33 of the Wangara campaign (Clarke et al., 1971). We have prescribed the initial wind and potential temperature profiles from the observations at 9h00, and used the observed heat flux at the surface and the geostrophic wind at the top of the model to drive our simulation. On that day, the CBL height varied from 250 m in the early morning to 1300 m at the end of the afternoon. With a turbulent velocity scale $w^* \approx 2 \text{ m s}^{-1}$, the integral time-scale z_i/w^* (computed with $z_i = 1000 \text{ m}$) is about 8 min. The height z_i of the CBL is defined by locating the altitude where the discretized second derivative of the average potential temperature profile is maximum. Fig. 1 shows that the modelled temperature profile is very close to the observations albeit slightly colder by about 1°C .

The quality of a LES model can be further estimated by its capacity to account for second order moments such as $\overline{w^2}$ or $\overline{\theta^2}$. Fig. 2 shows the simulated ratio $\overline{w^2}/w_*^2$ compared to the semi-empirical prediction for the CBL provided by mixed layer similarity (Stull, 2004), that is $1.8(z/z_i)^{2/3} \cdot (1 - 0.8(z/z_i))^2$. There is also good agreement between our LES model and theoretical similarity relation for second order moments.

2.2. Chemical model

The chemical component of our model is based on CHIMERE, a chemical model with 44 species and 120 reactions, including extensive photochem-

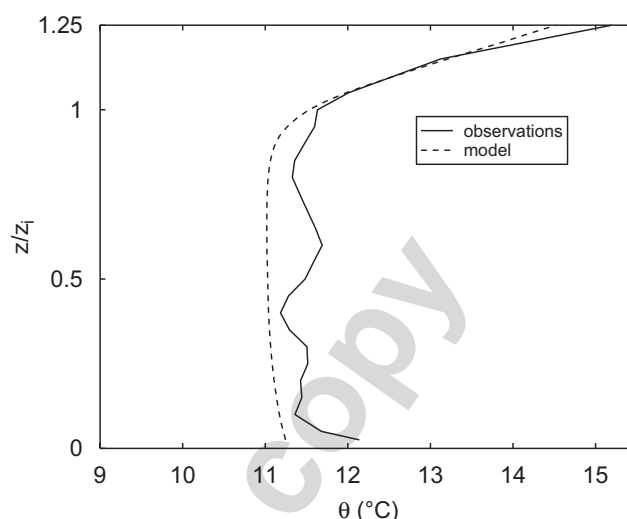


Fig. 1. Observed and computed profile of potential temperature in the CBL at 12h00 during day 33 of the Wangara campaign. The observed profile is a single sounding that exhibits convective bursts over a uniform background while the model profile is averaged over the domain and smooth.

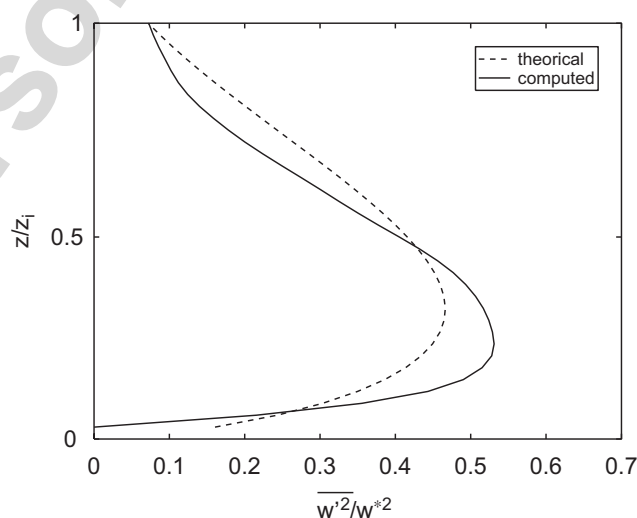


Fig. 2. Computed and theoretical profile of the ratio $\overline{w^2}/w_*^2$ at 11h00 during day 33 of the Wangara campaign.

istry, which is used for pollution simulation and forecast (Schmidt et al., 2001).

The framework of our simulations is a pure urban environment, implying the absence of biogenic emissions. Emissions in CHIMERE are retrieved from the 1999 EMEP database of anthropogenic emissions (Mylona, 1999). This database provides overall emissions for four classes of pollutants: NO_x , CO , SO_2 and NMVOC (non-methane volatile organic compound). The emissions rate for each of these classes is known for each SNAP (selected

nomenclature for air pollution) activity sector. Temporal variability for each class and each activity sector are provided by the IER (Institute for Energy Economics and Rational Use of Energy, University of Stuttgart; GENEMIS, 1994). Then the AEAT speciation (Passant, 2002) allows to divide the NMVOC family into model emitted NMVOC (C_2H_6 , NC_4H_{10} , C_2H_4 , C_3H_6 , APINEN, C_5H_8 , OXYL, HCHO, CH_3CHO , CH_3COE). We took the species emission for the Paris area as a boundary condition for our simulation, this area being representative of a heavily urbanized area, with high density road network and a variety of polluting industries. According to AIRPARIF data, road traffic is the major pollution contributor in Paris urban area for NO_x (52%) and CO (77%). It is also responsible for a big part of NMVOC emissions (32%). Industry emits most of the SO_2 (52%) and also contributes to NMVOC emissions (32%) and NO_x emissions (20%). Tertiary and residential pollution (mainly heating) accounts for 35% of SO_2 emissions and 19% of NMVOC emissions.

2.3. Damköhler number

From a set of chemical reactions, it is possible to define a characteristic production time-scale for species i

$$\frac{1}{\tau_{\text{prod}}} = \frac{1}{c_i} \sum_{j=1}^M \eta_{ij} k_j \prod_{l=1}^{N_j} c_l^{\beta_{lj}}, \quad (4)$$

where η_{ij} is the stoichiometric coefficient of species i in reaction j , k_j is the reaction rate of the equation j , β_{lj} is the reaction order of species l in reaction j , and M is the total number of reactions in which species i is engaged and the sum is over all the reactions for which species i is a product. We can in the same way define a destruction time-scale, τ_{dest} , where the sum in (4) is changed to a sum over all the equation in which the species i is a reactant. Usually those two time-scales are of comparable value, and hence only one time-scale $\tau_{\text{chem}} \approx \tau_{\text{prod}} \approx \tau_{\text{dest}}$ is characterizing the chemistry for a given specie. The Damköhler number is defined as the ratio

$$Da = \frac{\tau_c}{\tau_{\text{chem}}}$$

between the local turbulent time-scale τ_c and the chemical time-scale τ_{chem} .

When $Da \ll 1$ the chemistry is very slow compared to the local mixing, so the flow mixes all the

compounds as if they were inert and the generation of chemical products is then entirely limited by chemistry. When $Da \gg 1$ the chemical reactions are fast and a local chemical equilibrium is reached before the flow could perform any redistribution or as soon as chemical reactants are mixed together. In this case, the generation of chemical products is entirely limited by the dynamics. When $Da \simeq 1$, the chemical and dynamical time-scales are similar and one expects complex nonlinear effects of transport and mixing upon the chemical processes.

2.4. Segregation

As many chemical reactions are of second order, a widely used parameter to characterize turbulent effects is segregation defined as

$$s_{a,b} = \frac{\overline{a'b'}}{\overline{a}\overline{b}}, \quad (5)$$

where a and b are the concentrations for two species A and B . The bar represents a large-scale spatial average $\overline{a} = \int_D a(x) dx$, and the prime is the local deviation from this average. In our model the average is performed over the whole domain for each vertical layer.

Let us consider a simple second order reaction $A + B \rightarrow C$. For this simple chemical system, the production rate of species C is

$$\frac{d\bar{c}}{dt} = k(\overline{a}\overline{b} + \overline{a'b'}) = k\overline{a}\overline{b}(1 + s_{a,b}),$$

where k is the constant rate of the equation. The segregation coefficient is equal to the error made on the production rate by only taking into account the averaged values. Unlike the covariance $\overline{a'b'}/(\overline{a^2}\overline{b^2})^{1/2}$, segregation can take values between -1 and ∞ , the -1 limit being due to the positiveness of the concentrations.

3. Segregation factors

In this section and in the sequel, we use the complete model coupling the LES and the chemical solver, and simulate a urban area case on a $10 \text{ km} \times 10 \text{ km}$ domain. As a comparison, state-of-the-art large-scale pollution models at the time of this writing have a mesh-size of the order of $10\text{--}200 \text{ km}$. In the first experiment, denoted as the reference experiment in the sequel, our aim is to estimate the segregation when pollutant emissions are uniform at the ground.

Because of the periodicity of the boundary conditions in x and y , our model represents an infinite urbanized area. In order to avoid spurious buildup of pollutants, we impose a uniform decay rate for all species with a characteristic time-scale of 12 h, corresponding to a typical diurnal decay.

All the simulations are starting at $t = 9\text{h}00$ in the morning.

3.1. Sensitivity to the grid size

In order to test the sensitivity of our model to the variations of the mesh size, we have compared two experiments with $100 \times 100 \times 64$ grid points and $80 \times 80 \times 64$ grid points, that is with a mesh size of 100 and 125 m, respectively. Those two resolutions are both able to resolve updrafts and downdrafts for convective situations. Fig. 3 shows the ratio of chemical concentrations between the two experiments, averaged on the horizontal, for all species. The variation is weak inside the CBL ($z < z_i$) for all chemical species, since all ratio lie between 0.95 and 1.05 while the grid size has changed by a factor 1.25. Large sensitivity is seen above the boundary layer, due to the strong stability imposed there, which induces small time-scales and length scales that our model does not resolve, and to the very low concentrations in this region. This does not seem to impact on the CBL which is our domain of interest.

Fig. 4 compares the matrices of segregation at level 10 ($z = 250\text{ m}$) for each couple of species and for the two different resolutions, after 2 h of

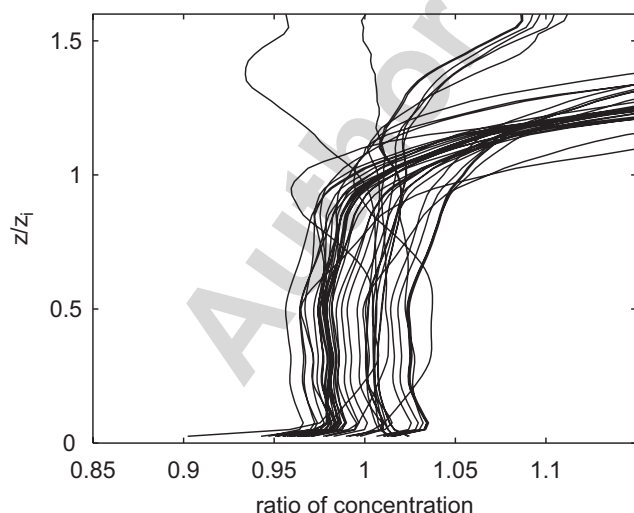


Fig. 3. Ratio of the concentration for each chemical compound between 80×80 and 100×100 experiments at $t = 12\text{h}30$.

simulation. Although segregation values are small for uniform emissions, it is important to observe that the two matrices are almost identical. In the sequel we will use only results from the $80 \times 80 \times 64$ grid.

3.2. Segregation sign

Fig. 4 shows that most instantaneous segregations are positive when emissions are uniform and when the initial environment is low-polluted. If pollutants are first considered as inert and are emitted, not necessarily uniformly, but with uniform composition over the domain, this composition is preserved by transport and diffusion which are linear processes in tracer concentration. Hence in (5), we have $a'/b' = \bar{a}/\bar{b}$ and segregation is positive. If chemistry is slow with respect to dynamics, segregation is still positive. This explains why most of the values in Fig. 4 are positive. The negative values in this case can only be explained by fast chemical reactions, in particular those involving chemical species not present within the emission but created within the turbulent boundary layer. Fig. 5 shows that the segregation between OH and NO is negative and fairly uniform within the depth of the CBL. These results are in agreement with Krol et al. (2000) who found weak and mainly positive segregations, of the same order as ours, when species are emitted uniformly at the ground.

When the emissions are not uniform, it has been shown in previous LES studies (Schuman, 1989; Sykes et al., 1994; Molemaker and Vilà-Guerau de Arellano, 1998) that segregation can reach significantly large negative values. In these studies based on a simple $A + B \rightarrow C$ chemical scheme, the species B is initially distributed within the domain and the species A emitted at the top boundary. Negative segregation then results from the fact that a local positive fluctuation in A leaves less B after the reaction has occurred. Another possibility, considered by Komori et al. (1991), which leads to negative segregation is that surface emissions are separated (some species emitted on one part of the surface at the ground, the other on the rest of the surface). In real cases, we know that most of the pollutants are due to road traffic. Our grid size is only twice the width of a major road, and mixing is performed at this horizontal scale within the surface layer over less than 1 min, that is much less than convective time-scale of updrafts in the boundary layer, $\tau_c = z_i/w^*$, which is of the order of 8 min, and

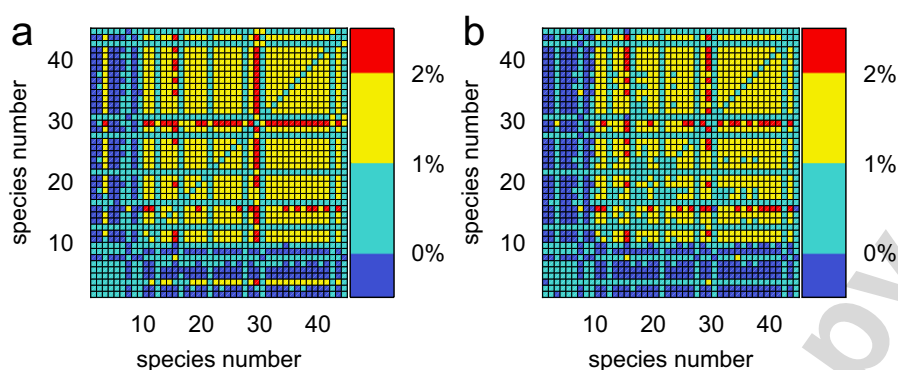


Fig. 4. Instantaneous segregation matrix for all the 45 species at level 10 (250 m) and $t = 11\text{h}00$, for the 80×80 grid (a) and for the 100×100 grid (b). The axis represent the 45 chemical species ranked as in Table 1, each cell displaying the segregation for one couple of species.

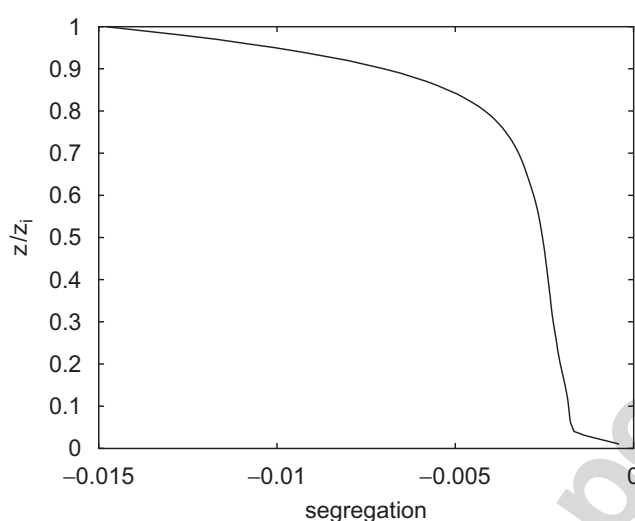


Fig. 5. Segregation between OH and NO as a function of altitude at 11h30.

the chemical time-scale of ozone production, which is of the order of 10 min. This approximation is likely to be incorrect for short-lived species which are generated in the surface layer but, nevertheless, we will not consider spatial separation of emission among pollutants in the sequel, and we will assume that they are always pre-mixed within the surface layer at the scale of the grid size before being lifted within updrafts as sketched in Fig. 6.

Sorting the chemical time-scales of our model in Table 1, we see that the first nine species with large Damköhler numbers are not affected by dynamics. The next nine species have chemical time-scales between 1 min and 1 h and are the most affected by local turbulent effects since they have Damköhler numbers of the order of 1. The last species in the list have time-scales that vary from 1 h for some volatile organic compounds to hundreds of hours for long-

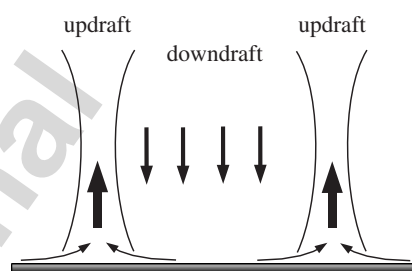


Fig. 6. Simplified representation of a convective boundary layer.

life constituents like CH_4 . All the compounds with characteristic time larger than one day behave like passive tracers and get mixed before they could react significantly.

Species with large Damköhler number, like OH are such that their chemical destruction and production time-scales are very small compared to τ_c over the whole vertical profile. A general property, first noticed by Galmarini et al. (1995) for a convective plume case, is that fast and reactive species combine to produce negative segregation. For instance, Fig. 4 shows that most of the species referenced as numbers greater than 14 that correspond for the majority to VOC (volatile organic compounds) are negatively correlated with OH (number 1) or HO_2 (number 6).

The reason is that during the first few hours of convection development, slowly varying species like VOC which are emitted at ground level are concentrated in the updrafts and more diluted elsewhere. On the contrary fast reacting species such as OH are not emitted but are produced from photochemistry and already well-mixed precursors all over the domain. As they are consumed by reactions with VOC, they are relatively less abundant inside the updrafts than outside. This can be seen on

Table 1
Chemical species (in the first column) ranked as a function of the Damköhler number (third COLUMN)

Species	3D/1D ratio	Da
OH	1.11	1.7×10^4
oRN1	0.99	1×10^4
NO ₃	0.72	7.1×10^3
CH ₃ COO	1.02	5.0×10^3
oPAN	0.96	2.4×10^4
HO ₂	0.99	2.2×10^3
obio	1.0	2.0×10^3
CH ₃ O ₂	1.01	2.0×10^3
oRO ₂	0.99	1.0×10^3
NO	0.79	18
NO ₂	0.67	9.2
O ₃	0.86	2.9
HONO	0.88	2.0
MEMALD	0.75	1.6
C ₃ H ₈	0.70	0.85
APINEN	0.90	0.60
obioH	0.92	0.59
CH ₃ COY	0.84	0.27
MAC	0.67	0.26
MGLYOX	0.75	0.20
oROOH	1.0	0.18
MVK	0.70	0.16
GLYOX	0.80	0.16
HCHO	0.74	0.15
CH ₃ CHO	0.71	0.13
CARNIT	0.47	0.13
PANH	0.99	0.13
OXYL	0.69	0.1
N ₂ O ₅	0.49	5.5×10^{-2}
CH ₃ O ₂ H	1.10	4.7×10^{-2}
PPA	1.11	3.4×10^{-2}
H ₂ O ₂	1.07	2.0×10^{-2}
NC ₄ H ₁₀	0.71	1.6×10^{-2}
toPAN	0.66	1.5×10^{-2}
CH ₃ COE	0.76	1.3×10^{-2}
ISNI	0.71	1.2×10^{-2}
C ₃ H ₆	0.68	8.3×10^{-3}
HNO ₃	0.75	2.2×10^{-3}
CO	0.72	1.6×10^{-2}
PAN	0.70	1.6×10^{-2}
C ₂ H ₆	0.72	1.3×10^{-2}
C ₂ H ₄	0.70	1.0×10^{-3}
CH ₄	0.57	2.6×10^{-4}
SO ₂	0.72	5.8×10^{-7}

The Damköhler number is calculated from the chemical time-scale of the species in the core of the CBL (level 20) at $t = 12\text{h}00$ and using the time-scale of updrafts as a dynamical time-scale. The second column shows the ratio of concentrations between the 3D and 1D experiment.

Fig. 7 where the highly concentrated OH areas are anticorrelated with the highly concentrated VOC areas, resulting into negative segregation between those two species (VOC concentration is defined as the sum over 32 species in our chemical system).

3.3. Segregation in the vertical

Fig. 8 shows that segregation varies a lot in the vertical: segregation is rather weak in the middle of the boundary layer (between $0.1z_i$ and $0.9z_i$), but strong values are obtained near the ground and at the top of the boundary layer. The strong values at the ground do not contradict the discussion of Section 3.2 since we only assume homogeneity at the mesh size. Wind advection vanishes at the surface and turbulent fluctuations are mostly governed by temperature fluctuations. The temperature fluctuations are also important at the top of the boundary layer. Indeed, the thickness of the two layers with larger segregation at the top and the bottom of the boundary layer are in good agreement with the thickness of the layers with large temperature fluctuation, as seen in Fig. 9. High $\langle\theta'^2\rangle$ values inside the CBL correspond to the less mixed regions, at the top and the bottom, whereas the overturning in the core of the CBL tends to smooth the θ' fluctuations. This is consistent with our finding that less dynamic mixing induces more segregation and agree with Krol et al. (2000) who found that the highest segregation values are obtained just above the surface.

Fig. 10 shows the evolution of the segregation profile between NO and O₃. First in the early development of the boundary layer the segregation values are of the order of a few percents through the vertical profile. After 1 h, segregation reaches a stationary profile in the lower part of the layer, with values of about 2% at the ground rapidly decreasing with altitude to values less than 1%.

3.4. Impact of segregation

In most cases seen in the previous section, segregation is of the order or less than 1% when emissions are homogeneous at the ground. It would be tempting to consider that effects of this magnitude are too small to be noticed and can be safely neglected. However, the small errors in the production rates can have a much larger effect on the average concentrations.

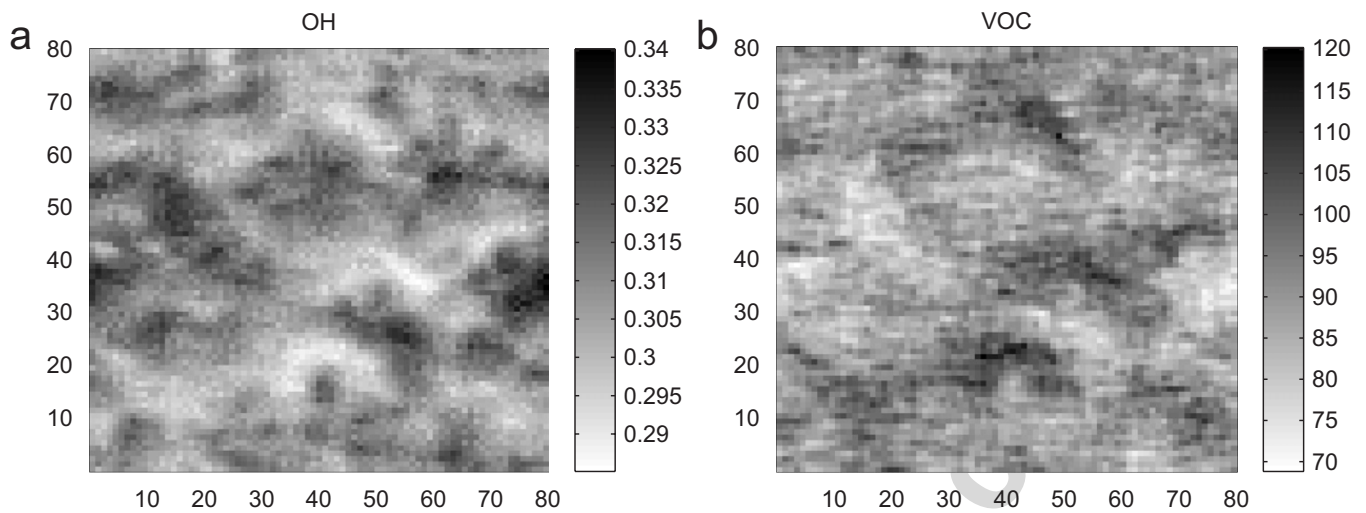


Fig. 7. Concentration field of OH (a) and VOC (b) at level 10 (250 m) and $t = 12\text{h}00$.

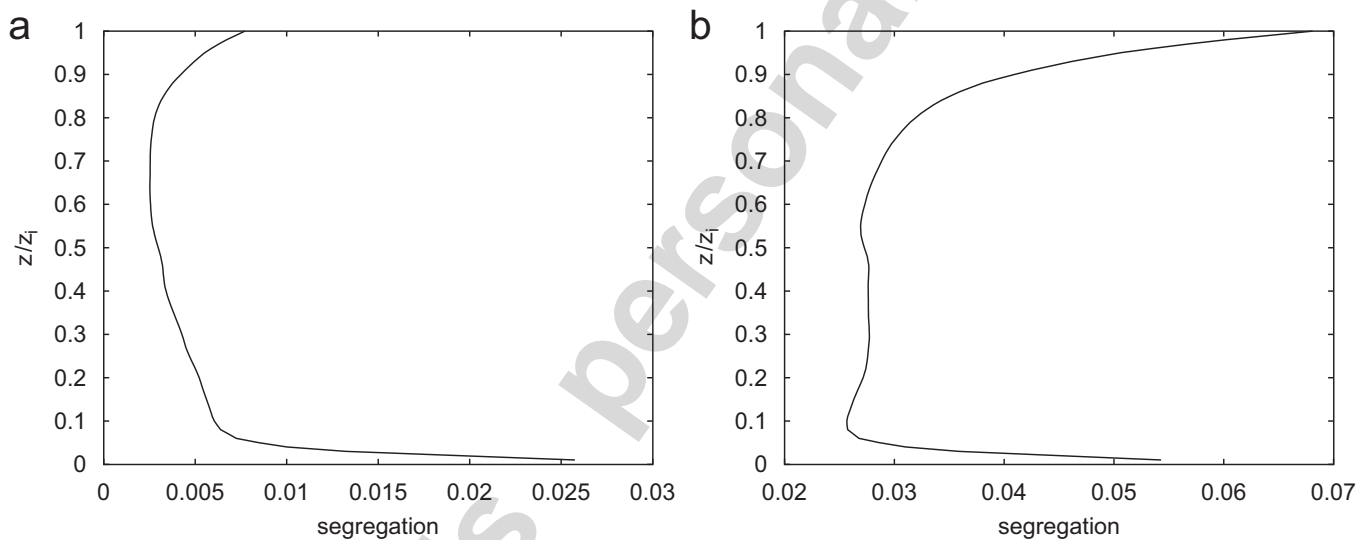


Fig. 8. Segregation as a function of altitude at $t = 11\text{h}30$, between O_3 and NO (a), C_5H_8 and NO_2 (b).

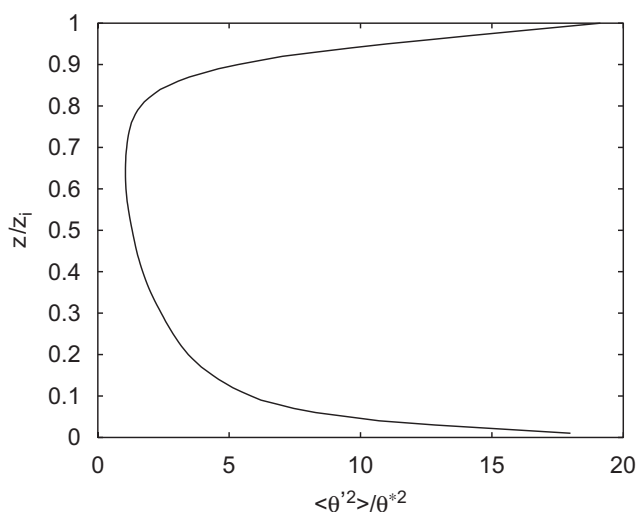
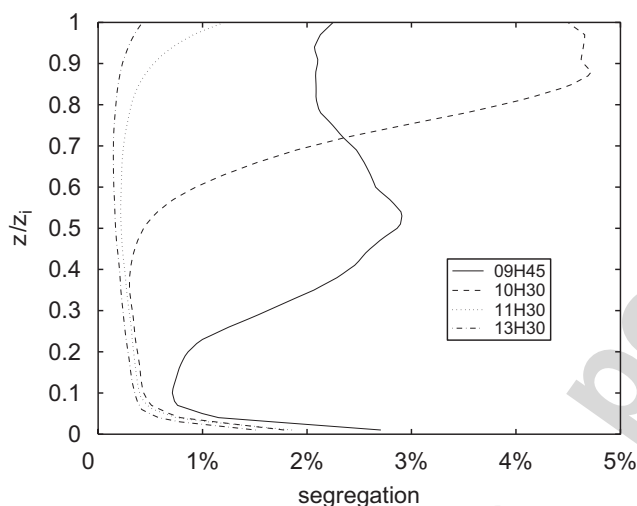
In order to estimate the effects of horizontal chemical segregation, we have performed a special experiment with the same turbulent transport as in the reference experiment described above but where the concentration of each species is set to the average within each level, at each time step. This approximation, denoted as the 1D model, is equivalent to an infinite horizontal diffusion and is meant to remove the effect of horizontal segregation, while preserving the vertical transport properties of the full 3D model. Fig. 11 compares the evolutions of four chemical species NO , NO_2 , OH and O_3 between the 3D (reference) and 1D model. In all cases, the concentrations are higher in the 3D model, with a difference of the order of 10% after 3 h for O_3 and OH and more

for NO and NO_2 . Thus, because of nonlinearities in the chemistry, a 1% segregation leads to much larger effects on the mean concentrations. Table 1 shows that species with small and mid Damköhler numbers are the most sensitive to segregation. Fast species are less sensitive, due to their lack of sensitivity to horizontal transport and diffusion and their small spatial correlation.

4. Segregation with heterogeneous emissions

4.1. Heterogeneity of the emissions

In this section, we consider a new experiment (SE1) where emissions are restrained to one half of

Fig. 9. $\langle \theta'^2 \rangle$ function of altitude at 11h30.Fig. 10. Temporal evolution of the segregation profile between NO and O₃.

the domain with a double rate with respect to the reference, so that the average emission of species over the whole domain is the same as before. The emission pattern for that experiment is sketched in Fig. 12. Since the geostrophic wind is parallel to the border between the two sub-domains, mean advection across the boundary of the two regions is due to the Ekman effect and has an amplitude of about 1 m s^{-1} . This transverse wind is able to sweep each sub-domain within the other in the course of a few hours, introducing a new time-scale for horizontal mixing, much longer than the convective time-scale, over which we expect the heterogeneity to play a role.

By simply assuming that fluctuations are doubled on one half-domain and set to zero on the second

half, we would expect to double segregation with respect to the reference experiment. However, the nonlinearities of the chemical reactions (Mathur et al., 1992; Vilà-Guerau de Arellano et al., 1993; Sillman et al., 1990) and the dynamical exchanges between the two subdomains considerably enhance the fluctuations and lead to much larger segregation than this simple prediction, as already observed by Krol et al. (2000) using localized emission with a Gaussian shape.

Indeed, Fig. 13 shows that segregation reaches high values at the beginning but decays to values akin to that of the homogeneous case during the course of the day, as a result of mixing within the boundary layer. Emissions are permanent but, as time evolves, the well-mixed charge of already released pollutants dominate over the inhomogeneities forced by new emissions. It is also remarkable, by comparing to Fig. 10 that the segregation profile is almost constant with altitude, without any sharp increase at the top and bottom boundaries. The reason is that fluctuations are now dominated by horizontal dynamical turbulent effects and not by temperature fluctuations and the distribution of updraft and downdraft like in the reference experiment.

During SE1 experiment, negative segregation between NO and O₃ is obtained after $t = 12\text{h}00$ while it is strongly positive during the first hours. As noted above, the sign of segregation depends a lot on the way the pollutants are emitted. Here, during the first two hours, O₃ is mainly produced where NO and other pollutants are emitted leading to positive segregation (see Section 3.2). At later stage, enough O₃ has accumulated and has been well-mixed within the domain to enter a regime where NO is oxidized by O₃ according to $\text{O}_3 + \text{NO} \rightarrow \text{NO}_2$ leading to the destruction of O₃ near pollutants sources. This regime leads to negative segregation as with a simple two-component reaction with one component distributed in the flow or emitted at the top, and the other one emitted at the ground (Vinueza and Vilà-Guerau de Arellano, 2005).

4.2. Covariance

The segregation of two species A and B can be written as a product of two terms,

$$I = \frac{\overline{ab}}{\bar{a}\bar{b}} = \frac{\overline{ab}}{\sigma_a\sigma_b} \frac{\sigma_a\sigma_b}{\bar{a}\bar{b}}, \quad (6)$$

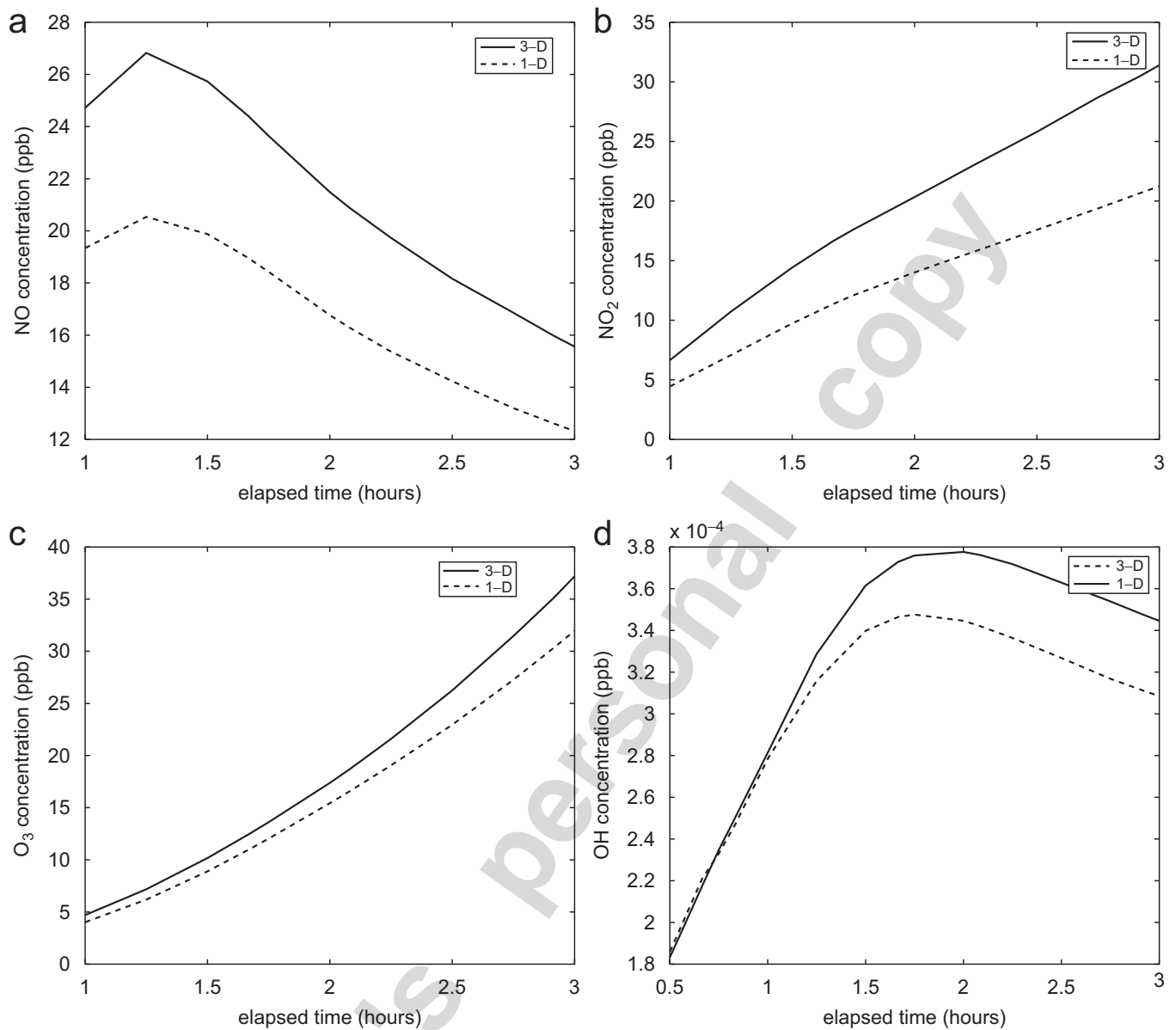


Fig. 11. Temporal evolution of chemical species at $z = 250$ m in the 1D (dashed) and 3D (solid) model: (a) NO; (b) NO₂; (c) O₃; and (d) OH.

where the first one is the correlation $\overline{ab}/\sigma_a\sigma_b$ and the second one is the ratio of correlation to mean concentrations $\sigma_a\sigma_b/\overline{ab}$. Here, the mean and standard deviations are computed over the whole domain.

The question addressed here is to attribute the evolution of segregation to one or the other term in (6). Vinuesa and Vilà-Guerau de Arellano (2005) assumed a constant correlation in the CBL. Indeed, Fig. 14 shows that correlation, which has maxima at the top and the bottom, is still strong a few hours after the beginning of the reference experiment. Hence the decay of segregation can only be due to the inverse product of the average concentration of

NO and O₃. However, in the SE1 experiment, Fig. 14 shows that correlation which is more uniform in the vertical changes a lot with time, with positive values at the beginning of the experiment turning to large negative values after 3 h. The assumption of a constant correlation in time is then only grossly valid for uniform emissions and does not apply to heterogeneous emissions.

4.3. Total ozone flux

We compare here the vertical flux of ozone for the homogeneous and heterogeneous emissions.

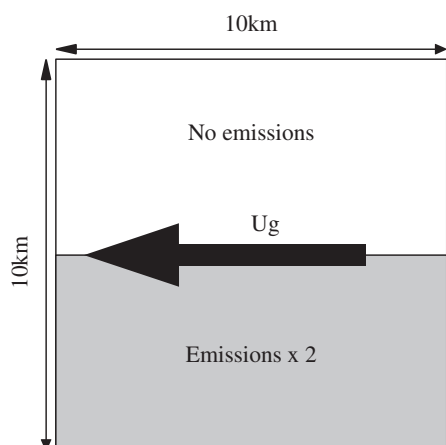


Fig. 12. Pattern of the emissions for experiment SE1. The arrow indicates the direction of the geostrophic wind.

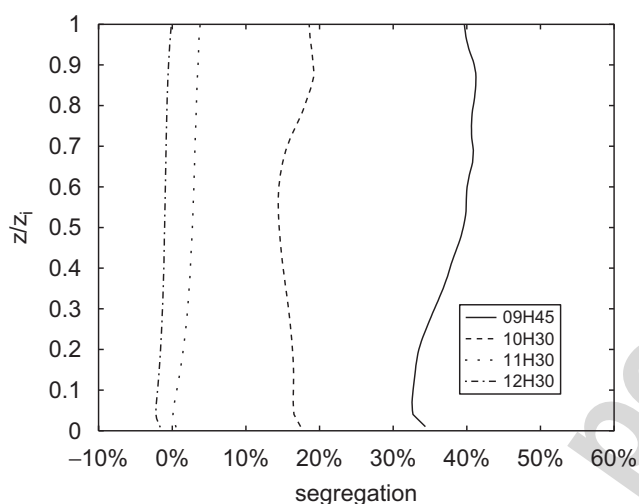


Fig. 13. Temporal evolution of segregation between NO and O₃ in the SE1 experiment.

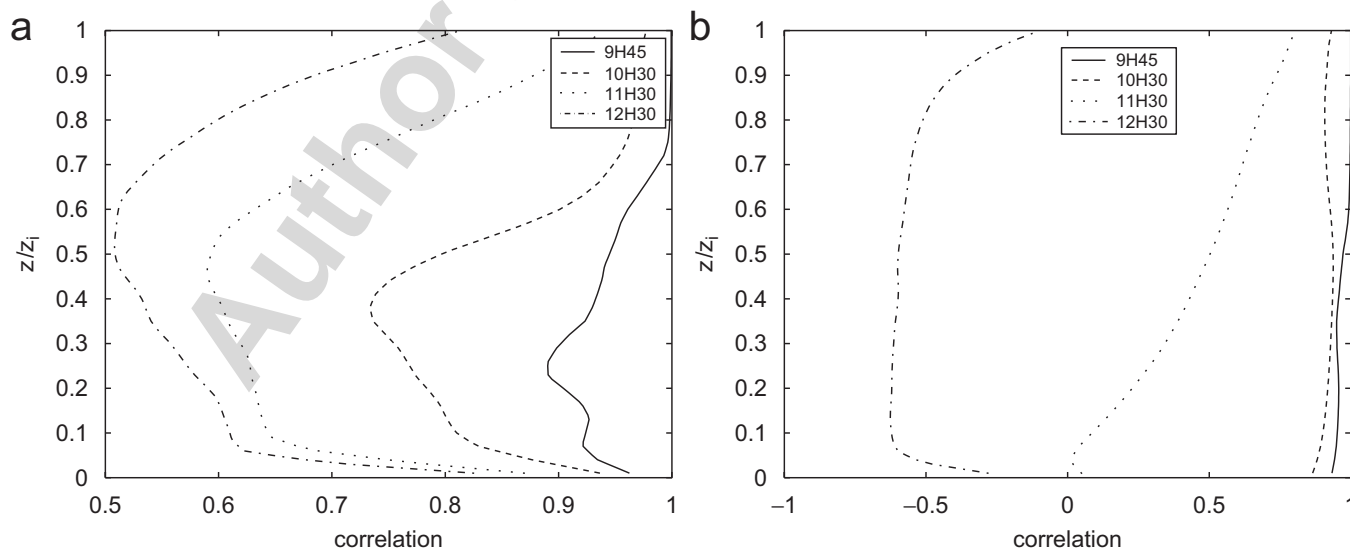


Fig. 14. Evolution of correlation between NO and O₃ for the reference experiment (a) and in the SE1 experiment (b).

Fig. 15 shows that, after 1 h, the ozone flux varies linearly in the first third of the CBL. The part of this slope with positive flux for $0.05 < z/z_i < 0.3$ corresponds to the levels where ozone is produced at that time. The smaller values for SE1 experiment is due to the larger segregation which reduces the reactivity and ozone production. After 2 h, Fig. 16, the linear profile extends up to $z/z_i \approx 0.8$, being positive above $z/z_i = 0.26$ for the reference experiment and $z/z_i = 0.37$ for SE1. The linear profile indicates a constant rate of ozone production (not taking into account chemical sources and sinks), that contributes to the ozone increase except at the top of the layer where ozone is mostly advected from below. The negative fluxes at the bottom of the CBL are due to deposition at the ground and ozone sink because of the reaction with NO (NO is strongly concentrated in the surface layer).

4.4. Mean concentrations

Fig. 17 shows that the difference in ozone between reference and SE1 experiment stays approximately constant with time between 1 and 3 h, and hence the relative difference decreases. Average NO and NO₂ (not shown) stay also very close.

However, Fig. 18 shows an important difference in OH between reference and SE1 experiment up to 3 h. This results looks at first sight paradoxical since the main source of OH is through ozone photolysis, and its main sink is by reaction with NO₂. The reason is that due to its short residence time, OH is strongly affected by fluctuations and segregation.

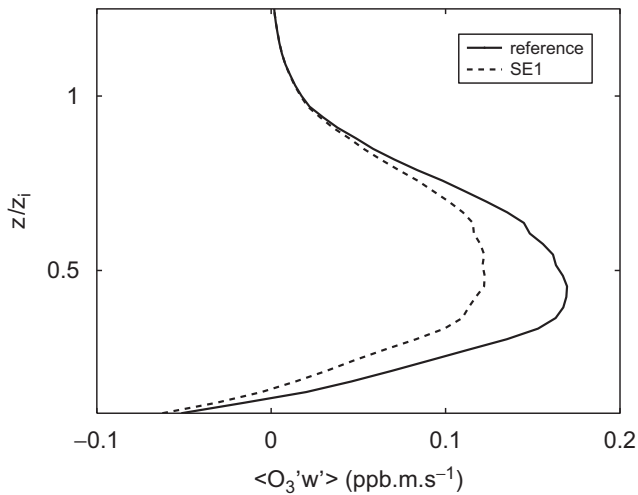


Fig. 15. Instantaneous O_3 vertical fluxes after 1 h of experiment.

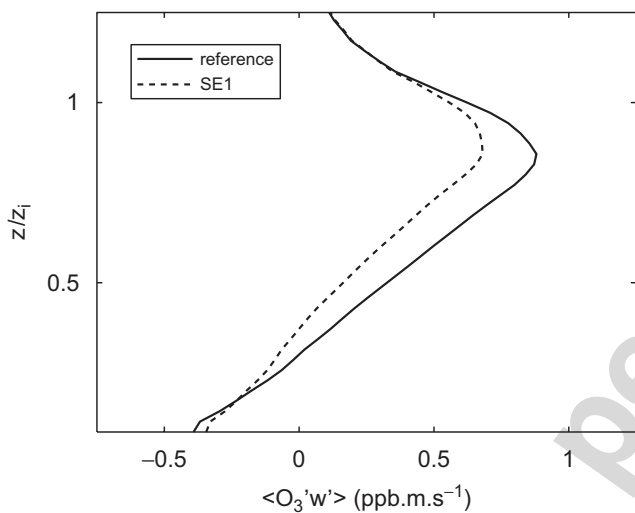


Fig. 16. Instantaneous O_3 vertical fluxes after 2 h of experiment.

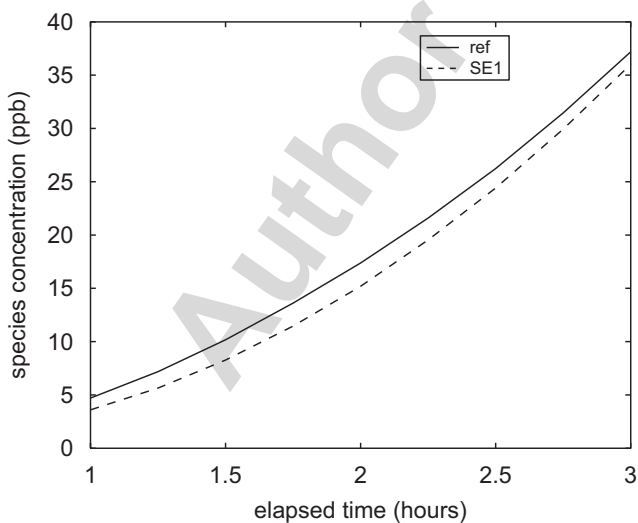


Fig. 17. Temporal evolution of O_3 for reference and SE1 experiments at level 10 (250 m).

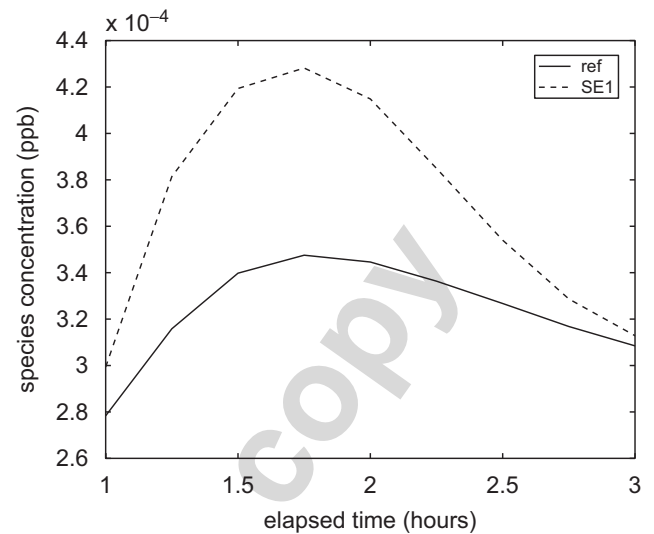


Fig. 18. Temporal evolution of OH concentration for reference and SE1 experiments.

Krol et al. (2000) found smaller differences in chemical species concentrations due to the fact they used a Gaussian emission pattern leading to smoother concentration gradients than in our case.

5. Effect of the distribution of heterogeneities

In order to test the sensitivity of the chemical system to the distribution of heterogeneities in the emissions, we have performed three experiments where the pattern of emissions is modified while keeping the whole emissions identical to the reference and SE1 experiments.

In the first two experiments of this section (SE2 and SE3), sketched in Fig. 19, we keep the same banded shape as in SE1. In experiment SE2, the emissions are concentrated over only 25% of the domain, that is in a band of 2.5 km width parallel to the geostrophic wind, but with a rate four times larger than in the reference experiment. In experiment SE3, the emissions are split in two parallel bands with twice the rate of the reference experiment.

The O_3 profile shown on Fig. 20 is quite affected during the first hour of SE2 since the concentration at $t = 10\text{h}00$ is nearly half the concentration of the reference experiment while SE3 value lies between SE1 and the reference experiment. At later time, the relative difference between reference and SE2 is decreasing as O_3 concentration is increasing. For VOC and NO_x , not shown, which are mostly

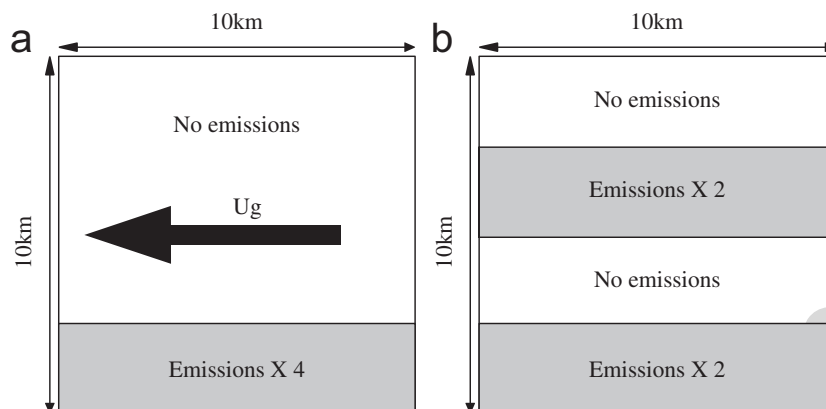


Fig. 19. Emission pattern for experiment SE2 (a) and SE3 (b). The arrow indicates the direction of the geostrophic wind and is omitted on the panel (b).

governed by total emissions, the differences are very small between the experiments. VOC–NO_x sensitivity studies (Hidy, 2000) show that O₃ production rate is considerably slowed down when VOC and NO_x are emitted at very high rates. As pollutants stay concentrated in the emission region over the first hours, the concentration of O₃ depends on the width of the emission band. After 1h30 of run, the averaged O₃ concentration is 25% less for the SE1 experiment compared to the reference experiment, and 39% less for the SE2 experiment compared to the reference experiment. As expected, the segregation is also considerably increased in SE2 experiment during the first hours, as shown in Fig. 21. SE3 experiment is much closer to the reference experiment, in term of averaged O₃ concentration (Fig. 20) and segregation (Fig. 21), with high segregation only during the first hour. After that time, due to the spreading of polluted areas, mixing occurs faster than in SE1 and segregation gets close to values of the reference experiment.

Our last experiment (SE4), sketched in Fig. 22, simulates a urban road network combining strips of high emission rates representing high traffic roads such as highways, and strips of less important emissions for less dense roads, which is four times denser but also with four times lighter emissions. The total emission rate is the same as in the previous experiments.

Fig. 23 shows that vertical profiles of segregation between NO and O₃ for this experiment are quite similar to the reference experiment (cf Fig. 10). The main differences are located between $z/z_i = 0.05$ and 0.5. At $t = 9\text{h}45$, the SE4 experiment exhibits less mixed pollutants than the reference, but surprisingly the segregation at $t = 10\text{h}30$ and

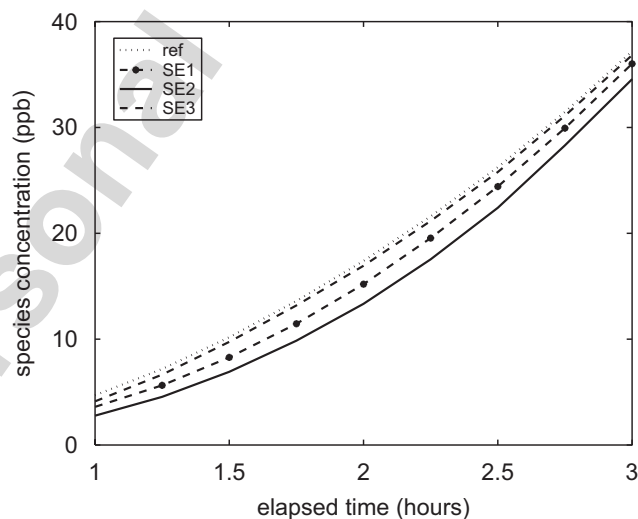


Fig. 20. Temporal evolution of O₃ concentration for the reference, SE1, SE2 and SE3 experiments.

11h30 is smaller than in the reference experiment. At later times, profiles from the two experiments are similar.

Indeed, after 3 h the concentration field above 250 m is completely similar to that of the reference experiment. There is also a close similarity in the distribution of OH, not shown, due to the fact that chemical compounds are well mixed above the surface layer, masking totally the effects of heterogeneities at the surface.

6. Summary and discussion

We have considered the impact of fluctuations at scales smaller than 10 km on ozone production by urban pollution, by coupling a LES and a realistic chemical model.

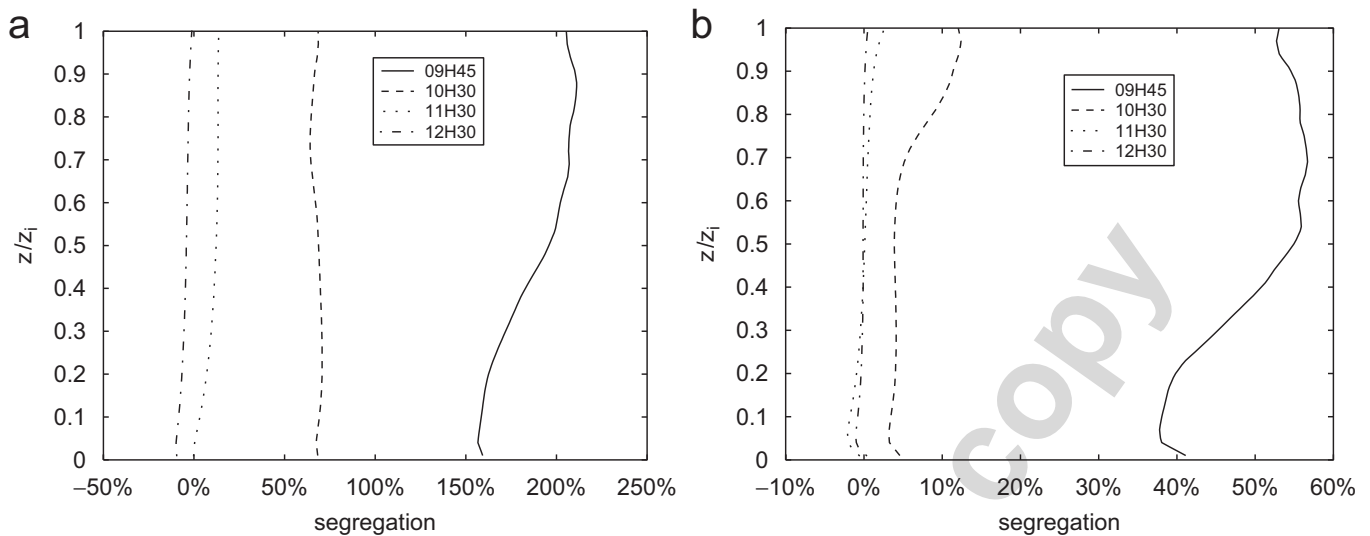


Fig. 21. Temporal evolution of segregation between NO and O₃: (a) SE2 experiment; (b) SE3 experiment.

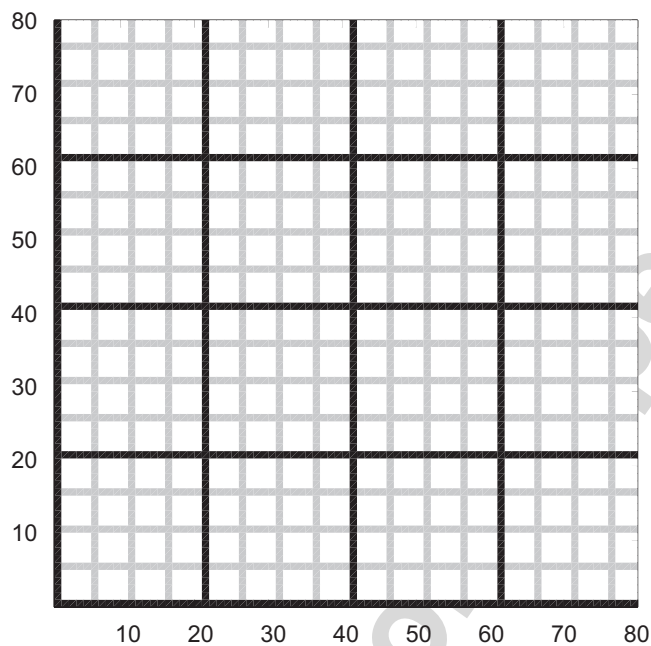


Fig. 22. Emissions at the ground for SE4 experiment. The black roads emissions rate is four times bigger than the grey roads emissions rate.

When emissions are uniform, the impact is small, either on average concentrations or on segregation for all couples of chemical species. Segregation culminates at about 10% during the first hour in this case and is less than 3% for most species after 2 h. Larger values at the top and the bottom of the CBL are due to larger temperature fluctuations and less vertical mixing. Negative segregation is obtained for chemical couples including a short-lived radical, otherwise segregation is positive.

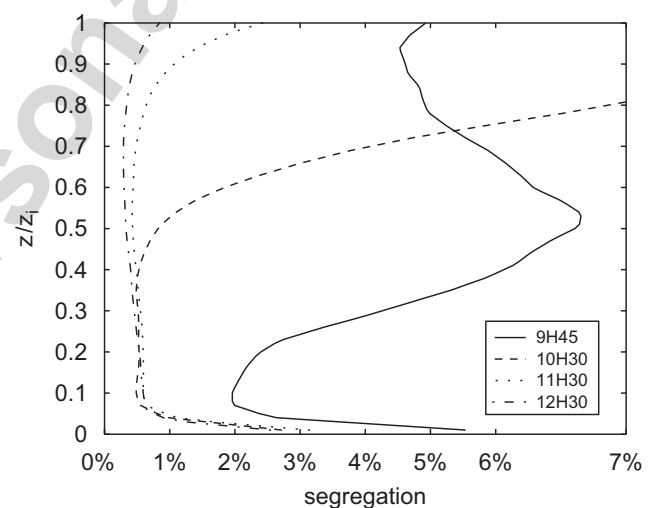


Fig. 23. Time evolution of segregation between NO and O₃ for experiment SE4.

When emissions are restricted to some areas at ground surface, much stronger segregations are observed which persist over at least 2 h. Segregation profiles are then uniform in the vertical as the dependency on temperature fluctuations and plumes is now dominated by the dependency on the distribution of ground emissions. The main differences between our model and previous coupled LES-chemistry models as in Krol et al. (2000), is that we used much more species and chemical reactions, and we prescribed sharp gradient emission patterns to restrict emissions over a small part of the domain. That leads to larger differences in terms of mean concentration for our simulations.

We proved that the amount of pollutants produced depends on the way the pollutants are emitted. Clearly the alternance of high and low emission rates favour segregation in the CBL. A measure is provided by the variance of emission rates normalized by the average emission, that we denote as ground segregation. However, this single parameter cannot characterize the effect of heterogeneities since the two experiments SE2 and SE3 yield different results with the same emission variance. Another key parameter seems to be the average size of gaps between the emission regions. A geometric measure is the ratio r of the length of the boundary between emission and non-emission regions (which could be defined in practice provided a given threshold) to the total area. For a given flow, this quantity provides an estimate of the capacity of emitted pollutants to mix within non-polluted air. Our experiments suggest that at constant r there is a relation between the ground segregation and the reduction in ozone production with respect to the reference experiment. Further experiments varying the geometrical distribution of the emissions are required to test the relevance of such parameters.

Acknowledgements

We acknowledge Robert Vautard and Matthias Beekmann for providing CHIMERE.

References

- Clarke, R., Dyer, A., Brook, R., Reid, D., Troup, A., 1971. The Wangara experiment: boundary layer data. Division of Meteorological Physics Technical Paper 19, CSIRO.
- Deardorff, J., 1972. Numerical investigation of neutral and unstable planetary boundary layers. *Journal of the Atmospheric Sciences* 29, 91–115.
- Deardorff, J.W., 1980. Stratocumulus-capped mixed layers derived from a three dimensional model. *Boundary-Layer Meteorology* 18, 495–527.
- Galmarini, S., Vilà-Guerau de Arellano, J., Duynkerke, P., 1995. The effect of micro-scale turbulence on the reaction rate in a chemically reactive plume. *Atmospheric Environment* 29, 87–95.
- Galmarini, J., Vilà-Guerau de Arellano, J., Duynkerke, P., 1997. Scaling the turbulent transport of chemical compounds in the surface layer under neutral and stratified conditions. *Quarterly Journal of the Royal Meteorological Society* 123 (537), 223–242.
- Gao, W., Wesely, M., 1994. Numerical modeling of the turbulent fluxes of chemically reactive trace gases in the atmospheric boundary layer. *Journal of Applied Meteorology* 33, 835–847.
- Hidy, G., 2000. Ozone process insights from field experiments. Part I: overview. *Atmospheric Environment* 34, 2001–2022.
- Kaimal, J., Businger, J., 1970. Case studies of a convective plume and a dust devil. *Journal of the Applied Meteorology* 9, 612–620.
- Komori, S., Hunt, J.C.R., Kanzaki, T., Murakami, Y., 1991. The effect of turbulent mixing on the correlation between two species and on concentration fluctuations in non-premixed reacting flows. *Journal of Fluid Mechanics* 228, 629–659.
- Krol, M., Molemaker, M., Vilà-Guerau de Arellano, J., 2000. Effects of turbulence and heterogeneous emissions on photochemically active species in the convective boundary layer. *Journal of Geophysical Research* 105, 6871–6884.
- Mathur, R., Peters, L., Saylor, R., 1992. Sub-grid representation of emission source clusters in regional air quality modeling. *Atmospheric Environment* 26, 3219–3236.
- Moeng, C.-H., 1984. A large-eddy-simulation model for the study of planetary boundary layer. *Journal of the Atmospheric Sciences* 41 (13), 2052–2062.
- Molemaker, M., Vilà-Guerau de Arellano, J., 1998. Control of chemical reactions by convective turbulence in the boundary layer. *Journal of the Atmospheric Sciences* 55 (4), 568–579.
- Mylona, S., 1999. EMEP emission data, status report 1999. Technical Report, EMEP/MS-C-W, EMEP, Oslo, Norway, Note 1/99.
- Passant, N., 2002. Speciation of UK emissions of NMVOC. Report AEAT/ENV/R/0545, AEA Technology, UK.
- Petersen, A., 2000. The impact of chemistry on flux estimates in the convective boundary layer. *Journal of the Atmospheric Sciences* 57, 3398–3405.
- Schmidt, H., Derognat, C., Vautard, R., Beekmann, M., 2001. A comparison of simulated and observed ozone mixing ratios for the summer of 1998 in Western Europe. *Atmospheric Environment* 35, 6277–6297.
- Schuman, U., 1989. Large-eddy simulation of turbulent diffusion with chemical reactions in the convective boundary layer. *Atmospheric Environment* 23, 1713–1729.
- Sillman, S., Logan, J.A., Wofsy, S.C., 1990. A regional scale model for ozone in the United States with subgrid representation of urban and power plant plumes. *Journal of Geophysical Research* 95, 5731–5748.
- Smagorinsky, J., 1963. General circulation experiments with the primitive equations. *Monthly Weather Review* 91, 99–165.
- Stull, B., 2004. An introduction to boundary layer meteorology. *Atmospheric and Oceanographic Sciences Library*. Kluwer Academic Publishers, Dordrecht.
- Sykes, R.I., Parker, S.F., Henn, D.S., 1994. Turbulent mixing with chemical reaction in the planetary boundary layer. *Journal of Applied Meteorology* 33, 825–834.
- Vautard, R., Beekmann, M., Roux, J., Gombert, D., 2001. Validation of a hybrid forecasting system for the ozone concentrations over the paris area. *Atmospheric Environment* 35, 2449–2461.
- Vilà-Guerau de Arellano, J., Duynkerke, P., 1995. Atmospheric surface layer similarity theory applied to chemically reactive species. *Journal of Geophysical Research* 100, 1397–1408.

Vilà-Guerau de Arellano, J., Duynkerke, P.G., Jonker, P.J., 1993. An observational study on the effects of time and space averaging in photochemical models. *Atmospheric Environment* 27, 353–362.

Vinuesa, J., Vilà-Guerau de Arellano, J., 2003. Fluxes and covariances of reacting scalars in the convective boundary layer. *Tellus B* 55 (4), 935–949.

Vinuesa, J., Vilà-Guerau de Arellano, J., 2005. Introducing effective reaction rates to account for the inefficient mixing of the convective boundary layer. *Atmospheric Environment* 9, 445–461.

Wilczak, J., Businger, J., 1983. Thermally indirect motions in the convective atmospheric boundary layer. *Journal of the Atmospheric Sciences* 40, 343–358.

Author's personal copy